Thermoelectromechanical effects in relaxed-shape graphene and band structures of graphene quantum dots

Sanjay Prabhakar,[1,*] Roderick Melnik,[1] Luis L. Bonilla,[2] and Shyam Badu[1]
[1]*The MS2Discovery Interdisciplinary Research Institute, M* [2]*NeT Laboratory, Wilfrid Laurier University, Waterloo, Ontario, N2L 3C5 Canada*
[2]*Gregorio Millan Institute, Universidad Carlos III de Madrid, 28911, Leganes, Spain*
(Received 23 January 2014; revised manuscript received 27 October 2014; published 17 November 2014)

We investigate the in-plane oscillations of relaxed-shape graphene due to externally applied tensile edge stress along both the armchair and zigzag directions. We show that the total elastic energy density is enhanced with temperature for the case of applied tensile edge stress along the zigzag direction. Thermoelectromechanical effects are treated via pseudomorphic vector potentials to analyze the influence of these coupled effects on the band structures of bilayer-graphene quantum dots. We report that the level crossing between the ground and first-excited states in the localized edge states can be achieved with accessible values of temperature. In particular, the level-crossing point extends to higher temperatures with decreasing externally applied tensile edge stress along the armchair direction. This kind of level crossing is absent in the states formed at the center of the graphene sheet due to the presence of threefold symmetry.

DOI: 10.1103/PhysRevB.90.205418 PACS number(s): 61.48.Gh, 62.23.Kn

I. INTRODUCTION

Miniaturization is one of the requirements to make electronic devices smaller and smaller. To fulfill this requirement, graphene-based electronic devices might provide a breakthrough alternative for the current state-of-the-art semiconductor industry. Graphene is a promising material to build electronic devices because of its unusual properties due to the Dirac-like spectrum of the charge carriers [1,2]. In addition, researchers around the world seek to make next-generation electronic devices from graphene because the material possesses high charge mobility. There is an opportunity to control the electronic properties of graphene-based structures by several different techniques, such as gate-controlled electric fields, magnetic fields, and to engineer the electromechanical properties via pseudomorphic gauge fields [3–11]. Recently, spin echo phenomena, followed by strong beating patterns due to rapid oscillations of quantum states along a graphene ribbon, have been investigated for realization of quantum memory at optical states in the far-infrared region for quantum information processing [12,13].

Graphene sheets designed to make next-generation electronic devices consist of surfaces that are not perfectly flat. The surfaces exhibit intrinsic microscopic roughening, the surface normal varies by several degrees and the out-of-plane deformations reach the nanometer scale [4,14–17]. Out-of-plane displacements without a preferred direction induce ripples in the graphene sheet [16,18–21], while in-plane displacements induced by applying suitable tensile edge stress along the armchair and zigzag directions lead to relaxed-shape graphene [9,32]. In experiments with graphene suspended on substrate trenches, there appear much longer and taller waves (close to the micron scale) directed parallel to the applied stress [9,22,32]. These long wrinkles are mechanically induced and we know that it is possible theoretically to corrugate an elastic membrane at absolute zero temperature. The mechanical deformation of a free-standing graphene sheet can be understood by applying suitable edge stress along the armchair and zigzag directions. The tensile forces that can be applied to the graphene sheet with a compressed elastic string are shown schematically in Fig. 1. In this paper, we show that intrinsic edge stresses can have a significant influence on the morphology of graphene sheets and substantially modify the band structures of graphene quantum dots. We present a model that couples the Navier equations, accounting for thermoelectromechanical effects, to the electronic properties of graphene quantum dots [23]. Here we show that the amplitude of the induced waves due to applied tensile edge stress along the armchair and zigzag directions increases with temperature and provides the level crossing in the localized edge states. This kind of level crossings is absent for the states formed at the center of the graphene sheet due to the presence of threefold symmetry induced by the pseudomorphic strain tensor.

II. THEORETICAL MODEL

The total thermoelastic energy density associated with the strain for the two-dimensional graphene sheet can be written as [10,20,24]

$$U_s = \tfrac{1}{2} C_{iklm}\varepsilon_{ik}\varepsilon_{lm} - \beta_{ik}\Theta(x,y)\varepsilon_{ik}\delta_{ik}, \tag{1}$$

where C_{iklm} is a tensor of rank four (the elastic modulus tensor), ε_{ik} (or ε_{lm}) is the strain tensor, and β_{ik} are the stress temperature coefficients. Also, $\Theta(x,y)$ is the distribution of temperature in the graphene sheet that can be found by solving Laplace's equation $\partial_i q_i = 0$, where $q_i = -\alpha_{ii}\partial_{x_i}\Theta$ with α_{ii} being the heat induction coefficients of graphene. Thus we write the Laplace's equation as

$$\alpha_{11}\partial_x^2\Theta + \alpha_{22}\partial_y^2\Theta = 0. \tag{2}$$

We suppose that the graphene sheet at boundary 4 (see Fig. 1) is connected to the heat bath of temperature $T(x)$ and that the three other boundaries 1, 2, and 3 are fixed at zero temperature. Thus, the exact solution of Laplace's equation can be

*Corresponding author: sprabhakar@wlu.ca

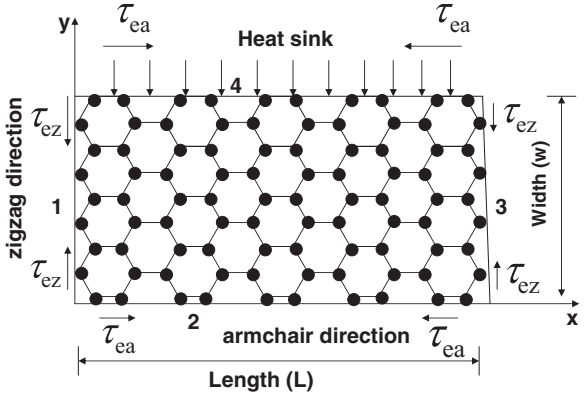

FIG. 1. Tensile stress applied along armchair and zigzag directions induces oscillation in strain tensor in graphene sheet. Boundary 4 is connected to the heat bath to investigate the influence of temperature on the strain tensor as well as on the band structures of graphene.

written as

$$\Theta(x,y) = \sum_{m=1}^{\infty} B_m \sinh\left(\frac{m\pi y}{L\sqrt{k_e}}\right) \sin\left(\frac{m\pi}{L}x\right), \quad (3)$$

where the constant B_m relates to the temperature of the thermal bath $T(x)$ as

$$T(x) = \sum_{m=1}^{\infty} B_m \sinh\left(\frac{m\pi w}{L\sqrt{k_e}}\right) \sin\left(\frac{m\pi}{L}x\right). \quad (4)$$

Here $k_e = \alpha_{22}/\alpha_{11}$, m is an integer, L is the length, and w is the width of the graphene sheet. The arbitrary constant B_m can be found by Fourier transforming Eq. (4):

$$B_m = \frac{2}{L\sinh[m\pi w/(L\sqrt{k_e})]} \int_0^L T(x) \sin\left(\frac{m\pi x}{L}\right) dx. \quad (5)$$

In Eq. (1), the strain tensor components can be written as

$$\varepsilon_{ik} = \tfrac{1}{2}\left(\partial_{x_k} u_i + \partial_{x_i} u_k + \partial_{x_k} h \partial_{x_i} h\right), \quad (6)$$

where u_i and h are the in-plane and out-of-plane displacements, respectively [20,25]. It is believed that the ripples in graphene have two different types of sources (see Figs. 1 and 3 of Ref. [26]). Both types of ripple waves are considered to be a sinusoidal function of position whose amplitude lies normal to the plane of the two-dimensional graphene sheet. The origin of first type of ripple results in relaxed-shape graphene (i.e., the displacement vector relaxes to the equilibrium position where the total elastic energy density is minimized) due to externally applied in-plane (along the x and y directions only) tensile edge stress [4]. Such kinds of ripples that can be seen in the form of relaxed-shape graphene occur in a fashion similar to leaves or torn plastic [27], where a buckling mechanism displaces only the carbon atoms near the edge of the graphene sheet [4,26]. While the origin of the second type of ripples results in height fluctuations throughout the graphene sheet due to adsorbed hydroxide molecules sitting on random sites of hexagon graphene molecules in the two-dimensional graphene sheet [28–30]. In this paper, we only consider the ripple waves induced by buckling mechanisms (i.e., $h = 0$) by applying tensile edge stress along the armchair and zigzag directions [4,31]. Hence the strain-tensor components for graphene in the two-dimensional (2D) displacement vector $\mathbf{u}(x,y) = (u_x, u_y)$ can be written as

$$\varepsilon_{xx} = \partial_x u_x, \quad \varepsilon_{yy} = \partial_y u_y, \quad \varepsilon_{xy} = \tfrac{1}{2}(\partial_y u_x + \partial_x u_y). \quad (7)$$

The stress tensor components $\sigma_{ik} = \partial U_s/\partial\varepsilon_{ik}$ for graphene can be written as [32]

$$\sigma_{xx} = C_{11}\varepsilon_{xx} + C_{12}\varepsilon_{yy} - \beta_{11}\Theta, \quad (8)$$

$$\sigma_{yy} = C_{12}\varepsilon_{xx} + C_{22}\varepsilon_{yy} - \beta_{22}\Theta, \quad (9)$$

$$\sigma_{xy} = 2C_{66}\varepsilon_{xy}. \quad (10)$$

In the continuum limit, elastic deformations of graphene sheets are described by the Navier equations $\partial_j\sigma_{ik} = 0$. Hence, the coupled Navier-type equations of thermoelasticity for graphene can be written as

$$\left(C_{11}\partial_x^2 + C_{66}\partial_y^2\right)u_x + (C_{12} + C_{66})\partial_x\partial_y u_y = \beta_{11}\Theta_x, \quad (11)$$

$$\left(C_{66}\partial_x^2 + C_{22}\partial_y^2\right)u_y + (C_{12} + C_{66})\partial_x\partial_y u_x = \beta_{22}\Theta_y, \quad (12)$$

where

$$\Theta_x = \sum_{m=1}^{\infty} \frac{m\pi B_m}{L} \sinh\left(\frac{m\pi y}{L\sqrt{k_e}}\right) \cos\left(\frac{m\pi}{L}x\right), \quad (13)$$

$$\Theta_y = \sum_{m=1}^{\infty} \frac{m\pi B_m}{L\sqrt{k_e}} \cosh\left(\frac{m\pi y}{L\sqrt{k_e}}\right) \sin\left(-\frac{m\pi}{L}x\right). \quad (14)$$

Now we apply the compressive tensile edge stresses through the boundaries of the graphene sheet (see Fig. 1) along the lateral directions and seek to establish the relationship between the waves generated due to applied tensile edge stresses and the in-plane displacement vector. More precisely, the mechanical deformation along the lateral direction of a graphene sheet can be understood by considering the effect of externally applied tensile edge stresses along the lateral direction in the form of compressed elastic string between which the 2D free-standing graphene sheet is clamped [9,24,32]. It is natural to expect that the longitudinal waves, generated by compressed elastic forces, travel along the direction of applied tensile edge stresses. Hence we might think that it is the sinusoidal function in the deformation of in-plane displacement vectors that correlate the geometric features of the longitudinal waves generated in the graphene sheet due to compressed elastic tensile edge stresses which finally turn the flat surface of the graphene sheet into relaxed-shape graphene in the form of torn plastic. Thus we assume the functional form of $\mathbf{u}(x,y)$ at boundary 2 of armchair as

$$u(x,0) = u_x = A\sin(kx), \quad (15)$$

where A is the amplitude and $k = 2\pi/\lambda$ with λ being the wavelength, while the total edge energy per unit length becomes [4]

$$U_e = \frac{1}{2}\tau_e\left(\frac{\partial u(x,0)}{\partial x}\right)^2 + \frac{1}{8}E_e\left(\frac{\partial u(x,0)}{\partial x}\right)^4, \quad (16)$$

where τ_e and E_e respectively denote the edge stress and the elastic modulus of the edge along the armchair direction of the graphene sheet. Thus, we write the total edge energy as $U_t = \int_0^L U_e dx$ and, by utilizing the condition $\partial U_t/\partial A = 0$, find the optimum amplitude of the waves along the armchair direction to be

$$A = \sqrt{\frac{2\tau_e[2kL + \sin(2kL)]}{E_e k^2[12kL + 8\sin(2kL) + \sin(4kL)]}}. \quad (17)$$

By considering $L = 1.5$ μm, $\tau_e = 4$ eV/nm, $E_e = 1000$ eV/nm, and $\lambda = 0.1$ to 1.5 μm, the amplitude A of the waves varies from 0.6 nm to 8.7 nm. This amplitude decreases exponentially as it moves into the graphene sheet along the y direction. Thus we assume $u(x,y) = A\sin(kx)\exp(-y/\ell)$, where ℓ is the penetration depth of the ripple waves, and write the total elastic energy of the graphene sheet as $\tilde{U} = U_t + \int_{x=0}^{L}\int_{y=0}^{\infty} U_s dx dy$. By considering $\partial\tilde{U}/\partial A = 0$, we find the functional form of the amplitude to be

$$2A\Gamma_1 + 4A^3\Gamma_2 - \Gamma_3 + \Gamma_4 = 0, \quad (18)$$

where

$$\Gamma_1 = \frac{k}{16}(2\tau_e + c_{11}\ell + c_{66}\ell)\{\sin(2kL) + 2kL\} - \frac{1}{16k\ell}(c_{22} + c_{66})\{\sin(2kL) - 2kL\} - \frac{1}{4}(c_{12} + c_{66})\sin^2(kL), \quad (19)$$

$$\Gamma_2 = \frac{E_e k^3}{32}\{12kL + 8\sin(2kL) + \sin(4kL)\}, \quad (20)$$

$$\Gamma_3 = \beta_{11}k\sum_{m=1}^{\infty}\frac{B_m}{2}\left\{\frac{\cos(m\pi + kL)}{m\pi + kL} + \frac{\cos(m\pi - kL)}{m\pi - kL} - \frac{2m\pi}{m^2\pi^2 - k^2L^2}\right\}\frac{m\pi L^2\ell^2\sqrt{k_e}}{m^2\pi^2\ell^2 - L^2\sqrt{k_e}}, \quad (21)$$

$$\Gamma_4 = \beta_{22}\sum_{m=1}^{\infty}\frac{B_m}{2}\left\{\frac{\sin(m\pi + kL)}{m\pi + kL} + \frac{\sin(m\pi - kL)}{m\pi - kL}\right\} \times \frac{m\pi L^2\ell\sqrt{k_e}}{m^2\pi^2\ell^2 - L^2\sqrt{k_e}}. \quad (22)$$

At absolute zero temperature (i.e., $\Gamma_3 = \Gamma_4 = 0$), the amplitude of the ripple waves obtained from Eq. (18) resembles the expression presented in Ref. [4]. Expressions similar to Eq. (18) can also be obtained for the optimum amplitude of the longitudinal waves along the zigzag direction by considering nonvanishing $u(0,y) = u_y = A\sin(ky)$ in Eq. (15) and replacing L by w in Eq. (17).

Now we turn to the analysis of the influence of strain on the electronic properties of graphene QDs formed in the graphene sheet with the application of a parabolic gate potential. In the continuum limit, by expanding the momentum close to the K point in the Brillouin zone, the Hamiltonian reads $H = \sum_k \Psi_k^\dagger \cdot H_k \cdot \Psi_k$. Here H_k is written as [3,6,36]

$$H_k = \begin{pmatrix} -U(x,y) & v_F P_+ & 0 & \frac{3\gamma_3 a P_-}{\hbar} \\ v_F P_- & -U(x,y) & \gamma_1 & 0 \\ 0 & \gamma_1 & U(x,y) & v_F P_+ \\ \frac{3\gamma_3 a P_+}{\hbar} & 0 & v_F P_- & U(x,y) \end{pmatrix}, \quad (23)$$

where $P_\pm = P_x \pm iP_y$ and $P = p - \hbar A$ with $p = -i\hbar\partial_x$ being the canonical momentum operator and $\mathbf{A} = \beta(\varepsilon_{xx} - \varepsilon_{yy}, \varepsilon_{xy})/a$ is the vector potential induced by the pseudomorphic strain tensor [25,37]. Also, a is the lattice constant, $v_F = 10^6$ m/s is the Fermi velocity, $\gamma_3 = 0.3$ eV corresponds to the interaction energy between two neighboring atoms A and B placed one under the other (see Ref. [3]), and $\beta = -\partial\ln t/\partial\ln a \approx 2$ with t being the nearest-neighbor hopping parameter. We assume a confining potential $U(x,y) = U_x + U_y$ that decays exponentially away from the edges into the bulk with penetration depths λ_1 or λ_2. Here we write $U(x)$ and $U(y)$ as [3,6]

$$U(x) = U_0\left\{\exp\left(\frac{-2x + L}{2\lambda_1}\right) + \exp\left(\frac{2x - L}{2\lambda_1}\right) - \xi\right\}, \quad (24)$$

$$U(y) = U_0\left\{\exp\left(\frac{-2y + w}{2\lambda_2}\right) + \exp\left(\frac{2y + w}{2\lambda_2}\right) - \xi\right\}, \quad (25)$$

where $\lambda_1 = L/2$, $\lambda_2 = w/2$, and ξ is a dimensionless constant. We can vary ξ to vary the band gap of graphene induced by gate potential.

III. RESULTS AND DISCUSSIONS

The schematic diagram of a two-dimensional graphene sheet in the computational domain is shown in Fig. 1. We applied the tensile edge stress along both the armchair and zigzag directions to create oscillations in the strain tensor of the graphene sheet. We used the multiphysics simulation and solved Navier's equations (11) and (12) via the finite element method to investigate the influence of thermoelectromechanical effects on the relaxed shape of graphene. For the waves along the armchair direction, we used the Neumann boundary conditions at sides 1 and 3 and employed Eq. (15) at sides 2 and 4, and vice versa for the zigzag direction. All reported results (Figs. 2–4) have been obtained for a 1.5×0.5 μm^2 graphene sheet that mimics the geometry of the experimentally studied structures in Ref. [11]. All parameters for our simulations are taken from Table I. For band-structure calculations (Figs. 5–7), we chose a 400×400 nm^2 graphene sheet.

Figure 2 shows the relaxed shape of graphene under applied tensile stress along the armchair direction. The variation in the amplitude of ripple waves, expressed in nanometers, is shown in the color bar [see Eq. (17)]. As can be seen in the color bar, the amplitude of the ripple waves in relaxed-shape graphene is enhanced with increasing wavelength, which is also supported analytically by Eq. (17). In Fig. 3, we investigate the influence of temperature on the strain tensor under an applied tensile edge stress along the armchair direction. Again, the oscillations in the strain tensor occur due to the applied tensile stress along the armchair direction that induces longitudinal waves and propagate along the armchair direction. We note that the increasing temperature from 0 K (upper panel) to room

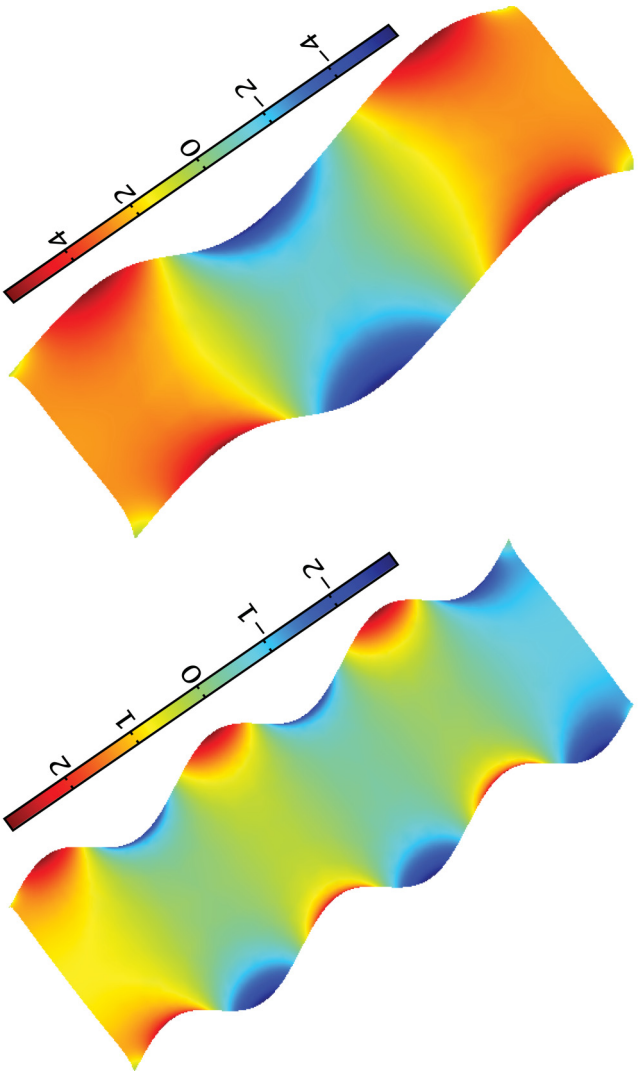

FIG. 2. (Color online) Relaxed shape of graphene due to applied tensile stress along armchair direction for (upper panel) $\lambda = 1\ \mu$m and (lower panel) $\lambda = 0.5\ \mu$m. Here we chose $T(x) = T_0 = 75$ K, $\tau_e = 4$ V/nm, $E_e = 1000$ eV/nm, and the dimension of the graphene sheet is taken to be $L \times w = 1.5 \times 0.5\ \mu$m^2. The longer and shorter sides are considered as the armchair and zigzag edges, respectively. The variation in the amplitude of the ripple waves, expressed in nanometers, is shown in the color bar.

temperature (lower panel) enhances the amplitude of the waves that eventually increase the magnetic field of the pseudomorphic vector potentials and allows us to investigate its influence in the band-structure calculation of graphene at Dirac points (for details, see Figs. 6 and 7). In Fig. 4, we investigate the total elastic energy density vs temperature. Even though the optimum values of the amplitudes of waves along the armchair and zigzag directions are exactly the same, the variation in the total free elastic energy density is enhanced for the case of applied tensile edge stress along the zigzag direction (dash-dotted line). This occurs because the graphene sheet along boundary 4 is connected to the heat reservoir that enhances the free elastic energy of the waves traveling along the zigzag direction.

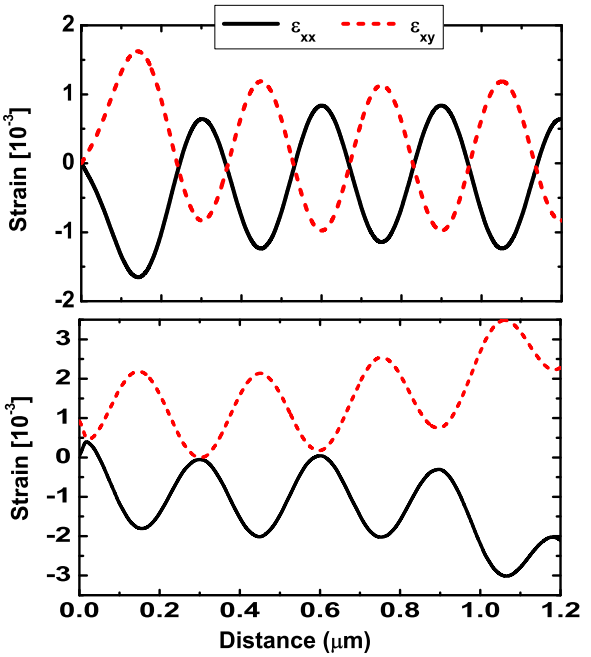

FIG. 3. (Color online) Oscillations in strain tensor due to applied tensile stress along the armchair direction at $y = w/2$ and temperature (upper panel) $T_0 = 0$ K and (lower panel) $T_0 = 300$ K. The parameters are chosen to be the same as in Fig. 2 but the wavelength $\lambda = 300$ nm.

Another important result of this paper is the study of the influence of thermomechanics on the band structure of bilayer-graphene QDs via pseudomorphic vector potentials. In Fig. 5, we plot several wave functions of the states of graphene QDs. It can be seen that, in addition to the localized states formed at the center of the graphene sheet, edge states are also present at the zigzag boundary. The localized edge states at the zigzag boundary can be seen due to the fact that the pseudomorphic vector potential originating from the

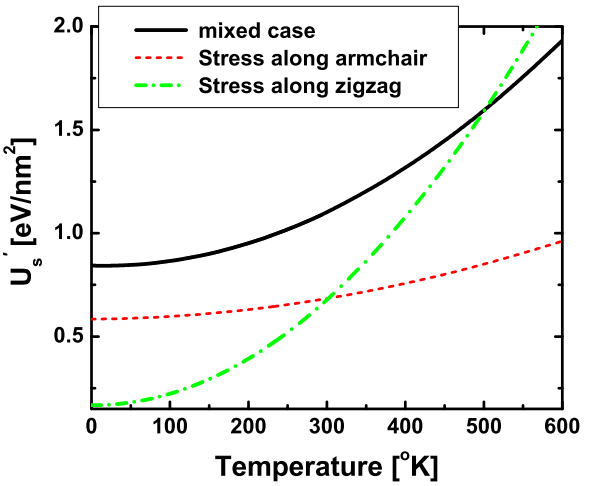

FIG. 4. (Color online) Free elastic energy density, $U_s' = 1/\tilde{A}(\int_\Omega U_s dxdy)$ with $\tilde{A} = Lw$ and Ω being the computational domain. For the mixed case, we applied the tensile edge stress along both the armchair and zigzag directions. The parameters are chosen to be the same as in Fig. 2.

TABLE I. The material constants for graphene used in our calculations are taken from Refs. [4,11,20,34,35].

Parameters	
C_{11} [N/m] = C_{22}	359.4
C_{12} [N/m]	41
C_{66} [N/m]	159.2
α_{11} [10^{-6} K^{-1}]	−7
α_{22} [10^{-6} K^{-1}]	−7
β_{11} [10^{-3} N/(mK)][a]	−2.8
β_{22}[10^{-3} N/(mK)][a]	−2.8

[a]The numerical values of the thermal coefficients β_{11} and β_{22} are obtained from expressions $\beta_{11} = C_{11}\alpha_{11} + C_{12}\alpha_{22}$ and $\beta_{22} = C_{12}\alpha_{11} + C_{22}\alpha_{22}$.

thermoelectromechanical effects generates a large magnetic field applied perpendicular to the two-dimensional graphene sheet. For example, considering $\mathbf{B} = \nabla \times \mathbf{A}$, we find $B_z = (2\pi\beta\varphi_0/a)\{\partial_x\varepsilon_{xy} - \partial_y(\varepsilon_{xx} - \varepsilon_{yy})\}$, where $\varphi_0 = \hbar/e$. Furthermore, by assuming sinusoidal functions of strain tensor (see Fig. 3) generated by applying tensile edge stress along the armchair direction, for example, $\varepsilon_{xx} = -\varepsilon_{xy} = \varepsilon_0 \sin(kx)$ and $\varepsilon_{yy} = 0$, where ε_0 is the amplitude of the strain tensor, we find $B_z = -B_0 \cos(kx)$, where $B_0 = 2\pi\varepsilon_0\beta k\hbar/(ae)$. By considering $\lambda = 300$ nm and $\varepsilon_0 = 10^{-3}$ (see Fig. 3, upper panel), we estimate $B_0 \approx 1.2$ T. Hence, such a large magnetic

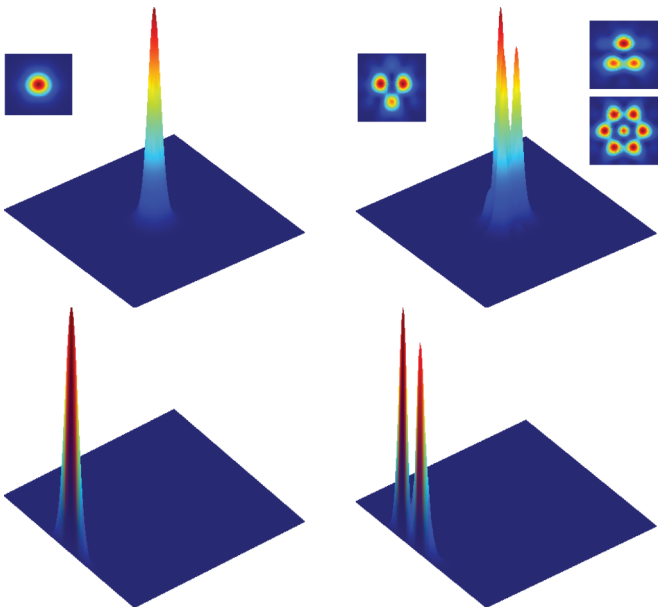

FIG. 5. (Color online) Demonstration of squared wave functions $|\Psi|^2$ formed by lateral confined potential $U(x,y)$ [see Eq. (23)] in $L \times w = 400 \times 400$ nm^2 graphene sheet. Upper panel shows the states formed at the center of the graphene sheet and lower panel shows the edge states formed at zigzag boundary 1 (see Fig. 1). Note that, in the upper panel, an unusual first-excited state wave function can be seen due to the presence of threefold symmetry in graphene. For eigenvalues, see Fig. 6. For electromechanical parts, we chose $\tau_e = 45$ eV/nm, $E_e = 1000$ eV/nm, and $T_0 = 5$ K that mimic the experimentally reported values in Ref. [33]. For band-structure calculations, we chose $U_0 = 0.2$ eV, $\lambda_1 = \lambda_2 = 200$ nm, and the dimensionless parameter $\xi = 1.97$.

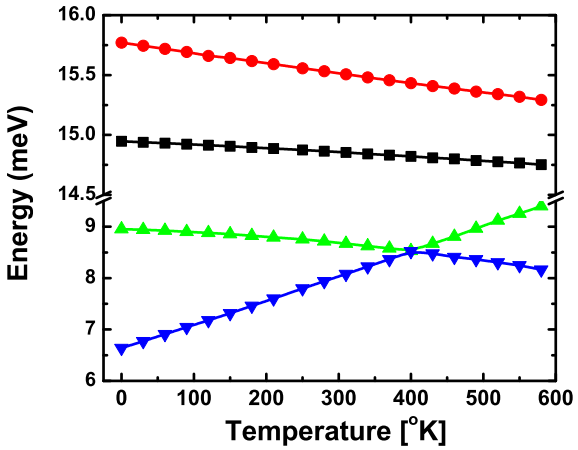

FIG. 6. (Color online) Ground- and first-excited-state eigenenergies formed at the center of the graphene sheet (diamonds and circles) and at the edge of boundary 1 (triangles pointing up and triangles pointing down) vs temperature for the case $\tau_e = 45$ eV/nm along the armchair direction. It can be seen that the level crossing between the ground- and first-excited-state edge energy occurs at $T = 400$ K. The parameters are chosen to be the same as in Fig. 5.

field along the z direction originating from electromechanical effects induces a persistent current that flows toward the edge of the graphene. As a result, a positive (negative) dispersion in the electron-like (hole-like) states is induced at the zigzag edge (see also Fig. 4 of Ref. [38]) and the localized electron-hole-state wave functions drift towards and over the edge of the graphene sheet [38–40]. Hence, the wave functions that are pressed against the edge finally turn into the localized edge current carrying states [38–41]. Similar localized edge states are also shown in Fig. 2(d) of Ref. [38]. Furthermore, by utilizing tight binding and continuum models, the authors in Ref. [41] have shown that the tunneling effect at the interface between the internal and external regions of the dots can be avoided and, consequently, the charge carriers are confined at the zigzag edge [see, for example, Eq. (11) and

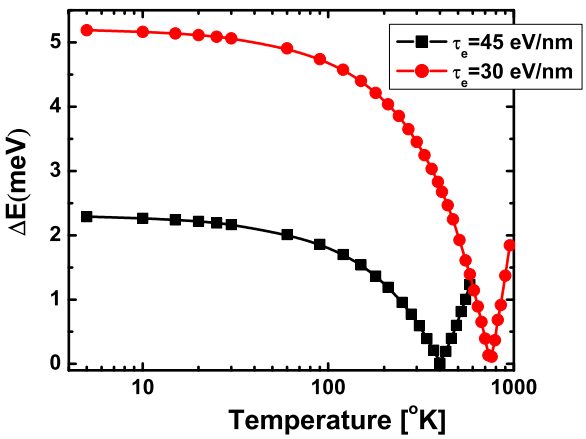

FIG. 7. (Color online) Edge-energy difference $\Delta E = E_1 - E_2$ for the states at boundary 1 vs temperature. We can see that the level-crossing point extends to larger temperatures with decreasing externally applied tensile edge stress along the armchair direction.

left panel of Fig. 6 of Ref. [41]]. Such localized edge states, shown in the lower panel of Fig. 5 in this paper, are highly sensitive to the applied tensile edge stress along the armchair and zigzag directions. We observe threefold symmetry in the first-excited-state wave function (see inset plot of Fig. 5) of graphene that is agreed with the experimentally reported results [see Fig. (4) of Ref. [42]] and previously reported theoretical results (see Ref. [43]). In Fig. 6, we find the level crossing at $T = 400$ K due to the fact that the edge energy difference between the ground and first-excited states decreases with increasing temperature. This level-crossing point extends to higher temperatures with decreasing tensile edge stress (see Fig. 7). We analyzed why the level-crossing point can be seen on the edge states but cannot be seen on the localized states formed at the center of the graphene sheet. The reason is that the graphene sheet at boundary 4 is connected to the heat reservoir. Hence, the energy difference between the ground and first-excited states decreases with increasing temperature. As a result, we find the level crossing in the edge states to be at the zigzag boundary with the accessible values of temperatures. The energy difference between the ground and first-excited states formed at the center of the graphene sheet also decreases with increasing temperature (see Fig. 6). However, such energy states do not meet each other with any practically applicable values of the temperature due to the absence of twofold symmetry in graphene. In fact, the pseudomorphic fields induced by the strain tensor affect the graphene charge carriers and produce a threefold symmetry in the wave function of the two-dimensional graphene sheet (see inset plot of Fig. 5). The symmetry of the pseudomorphic fields is determined by the corresponding symmetry of the strain field. For example, a uniform pseudomorphic field requires a special strain field distorted with threefold symmetry [17,42].

IV. CONCLUSION

To conclude, we developed a model which allows us to investigate the influence of temperature on the relaxed shape of a graphene sheet as well as in the QDs that are formed in a two-dimensional graphene sheet with the application of gate potentials. We showed that the variation in the total free elastic energy density is enhanced with temperature for the case of applied tensile edge stress along the zigzag direction. We treated the strain induced by an applied tensile edge stress along the armchair and zigzag directions as a pseudomorphic vector potential and showed that the level-crossing point between the ground and first-excited edge states at the zigzag boundary extends to higher temperatures with decreasing tensile edge stress. Such level crossings are absent in the states formed at the center of the graphene sheet due to the presence of threefold symmetry.

ACKNOWLEDGMENTS

This work was supported by the NSERC and CRC programs (Canada). The authors acknowledge the Shared Hierarchical Academic Research Computing Network (SHARCNET) community and Dr. P. J. Douglas Roberts for his assistance and technical support.

[1] K. S. Novoselov, A. K. Geim, S. V. Morozov, D. Jiang, Y. Zhang, S. V. Dubonos, I. V. Grigorieva, and A. A. Firsov, Science **306**, 666 (2004).
[2] K. S. Novoselov, D. Jiang, F. Schedin, T. J. Booth, V. V. Khotkevich, S. V. Morozov, and A. K. Geim, Proc. Natl. Acad. Sci. USA **102**, 10451 (2005).
[3] A. H. Castro Neto, F. Guinea, N. M. R. Peres, K. S. Novoselov, and A. K. Geim, Rev. Mod. Phys. **81**, 109 (2009).
[4] V. B. Shenoy, C. D. Reddy, A. Ramasubramaniam, and Y. W. Zhang, Phys. Rev. Lett. **101**, 245501 (2008).
[5] S.-M. Choi, S.-H. Jhi, and Y.-W. Son, Phys. Rev. B **81**, 081407 (2010).
[6] P. A. Maksym and H. Aoki, Phys. Rev. B **88**, 081406 (2013).
[7] W. Bao, K. Myhro, Z. Zhao, Z. Chen, W. Jang, L. Jing, F. Miao, H. Zhang, C. Dames, and C. N. Lau, Nano Lett. **12**, 5470 (2012).
[8] Z. Yan, G. Liu, J. M. Khan, and A. A. Balandin, Nat. Commun. **3**, 827 (2012).
[9] E. Cadelano, P. L. Palla, S. Giordano, and L. Colombo, Phys. Rev. Lett. **102**, 235502 (2009).
[10] E. Cadelano and L. Colombo, Phys. Rev. B **85**, 245434 (2012).
[11] W. Bao, F. Miao, Z. Chen, H. Zhang, W. Jang, C. Dames, and C. N. Lau, Nat. Nanotechnol. **4**, 562 (2009).
[12] S. Prabhakar, R. Melnik, L. L. Bonilla, and J. E. Raynolds, Appl. Phys. Lett. **103**, 233112 (2013).
[13] M. B. Belonenko, A. V. Zhukov, K. Nemchenko, S. Prabhakar, and R. Melnik, Mod. Phys. Lett. B **26**, 1250094 (2012).
[14] M. H. Gass, U. Bangert, A. L. Bleloch, P. Wang, R. R. Nair, and A. K. Geim, Nat. Nanotechnol. **3**, 676 (2008).
[15] J. C. Meyer, A. K. Geim, M. I. Katsnelson, K. S. Novoselov, T. J. Booth, and S. Roth, Nature (London) **446**, 60 (2007).
[16] L. L. Bonilla and A. Carpio, Phys. Rev. B **86**, 195402 (2012).
[17] F. Guinea, M. I. Katsnelson, and A. K. Geim, Nat. Phys. **6**, 30 (2010).
[18] M. Gibertini, A. Tomadin, M. Polini, A. Fasolino, and M. I. Katsnelson, Phys. Rev. B **81**, 125437 (2010).
[19] H. Wang and M. Upmanyu, Phys. Rev. B **86**, 205411 (2012).
[20] A. Carpio and L. L. Bonilla, Phys. Rev. B **78**, 085406 (2008).
[21] P. San-Jose, J. González, and F. Guinea, Phys. Rev. Lett. **106**, 045502 (2011).
[22] E. Cerda and L. Mahadevan, Phys. Rev. Lett. **90**, 074302 (2003).
[23] K. V. Zakharchenko, M. I. Katsnelson, and A. Fasolino, Phys. Rev. Lett. **102**, 046808 (2009).
[24] L. D. Landau and E. M. Lifshitz, *Theory of Elasticity* (Pergamon Press Ltd., Oxford, 1970).
[25] F. de Juan, J. L. Mañes, and M. A. H. Vozmediano, Phys. Rev. B **87**, 165131 (2013).
[26] R. C. Thompson-Flagg, M. J. B. Moura, and M. Marder, Europhys. Lett. **85**, 46002 (2009).
[27] E. Sharon, B. Roman, M. Marder, G.-S. Shin, and H. L. Swinney, Nature (London) **419**, 579 (2002).

[28] T. J. Echtermeyer, M. C. Lemme, M. Baus, B. N. Szafranek, A. K. Geim, and H. Kurz, IEEE Electron Device Lett. **29**, 952 (2008).
[29] A. Fasolino, J. H. Los, and M. I. Katsnelson, Nat. Mater. **6**, 858 (2007).
[30] J. Moser, A. Verdaguer, D. Jimenez, A. Barreiro, and A. Bachtold, Appl. Phys. Lett. **92**, 123507 (2008).
[31] Our model is only valid for a case where ripple waves can be generated via externally applied tensile edge stress where the amplitude of the ripple waves, which lie normal to the plane of two-dimensional graphene sheet, decay exponentially as they move into the graphene sheet, similar to Ref. [4] and Fig. 1 of Ref. [26]. For a case where the ripple waves can be observed throughout the sample of the graphene sheet, similar to Ref. [27] of Fig. 2, we can not assume $h = 0$ in Eq. (6), so substantial improvement of the developed model is necessary for such a scenario.
[32] J. Zhou and R. Huang, J. Mech. Phys. Solids **56**, 1609 (2008).
[33] C. Lee, X. Wei, J. W. Kysar, and J. Hone, Science **321**, 385 (2008).
[34] L. Shen, H.-S. Shen, and C.-L. Zhang, Comput. Mater. Sci. **48**, 680 (2010).
[35] D. Yoon, Y.-W. Son, and H. Cheong, Nano Lett. **11**, 3227 (2011).
[36] V. Krueckl and K. Richter, Phys. Rev. B **85**, 115433 (2012).
[37] F. Guinea, B. Horovitz, and P. Le Doussal, Phys. Rev. B **77**, 205421 (2008).
[38] A. H. Castro Neto, F. Guinea, and N. M. R. Peres, Phys. Rev. B **73**, 205408 (2006).
[39] X.-G. Wen, Int. J. Mod. Phys. B **06**, 1711 (1992).
[40] A. Vikstroöm, arXiv:1407.5018.
[41] M. Zarenia, A. Chaves, G. A. Farias, and F. M. Peeters, Phys. Rev. B **84**, 245403 (2011).
[42] N. N. Klimov, S. Jung, S. Zhu, T. Li, C. A. Wright, S. D. Solares, D. B. Newell, N. B. Zhitenev, and J. A. Stroscio, Science **336**, 1557 (2012).
[43] D. Moldovan, M. Ramezani Masir, and F. M. Peeters, Phys. Rev. B **88**, 035446 (2013).